World Scientific
www.worldscientific.com

Numerical Simulation of Viscous Flows Around a Surface Combatant Model at Different Drift Angles Using Overset Grids

Jianhua Wang, Zhenghao Liu and Decheng Wan*

Computational Marine Hydrodynamics Lab (CMHL)
State Key Laboratory of Ocean Engineering
School of Naval Architecture, Ocean and Civil Engineering
Shanghai Jiao Tong University, Shanghai, P. R. China
*dcwan@sjtu.edu.cn

Viscous flows around ship hull is of great complexity, and when the ship is advancing with drift angles, the flow field can be more complicated. In this paper, the viscous flow field around an obliquely towed surface combatant DTMB 5512 is computed using the unsteady Reynolds-averaged Navier–Stokes (URANS) method. The numerical simulations are carried out by the in-house CFD solver naoe-FOAM-SJTU, which is developed on the open source platform OpenFOAM. To refine local grids and simulate dynamic ship motions, the overset grid approach is applied. Grid convergence study is first performed at straight-ahead towed condition with three sets of grid number and the results show monotonically convergence. Six different drift angles for the DTMB 5512 model at Froude number of 0.28 are simulated and the predicted hydrodynamic forces and flow field are presented. During the simulation, the ship hull is free to trim and sinkage at a free surface environment. As for straight-ahead towed condition, the total resistance coefficient and flow field, i.e., wave pattern and wake region, between this work and the experiment are compared. Both force coefficients and flow field show good agreement with the available experimental data. For oblique towed conditions, the lateral force, yaw moment and the derived hydrodynamic derivatives are also presented and compared with the experimental results. The variation of wave pattern and wake region at different drift angles are presented and analyzed. The results show that the current approach can be an effective tool to predict the viscous flows and hydrodynamic loads for oblique towed ships.

Keywords: Surface combatant; naoe-FOAM-SJTU solver; viscous flow field; overset grid; drift angle.

---

*Corresponding author.

1. Introduction

Good maneuvering behavior of a ship is essential to keep its navigational safety. In the last few decades, several standards have been developed by the International Maritime Organization (IMO) for ship maneuverability. The hydrodynamic performance acting on an advancing ship with drift angles is of paramount importance in the ship maneuverability. As we know, when a ship is traveling with drift angles, the lateral forces as well as yaw moments acting on the hull will push the ship sideways. The effect of drift angle has significant influence on ship resistance, propulsion, maneuverability and stability. Thus, it is essential to investigate the flow characteristics around ship hull at different drift angles to better understand the hydrodynamic performance. Up to now, many researchers have studied the hydrodynamic performance and flow field of different types of oblique towed vessels.

Previous investigations are mostly relied on model tests, where static and dynamic planar motion mechanism (PMM) tests are commonly applied. These tests can be feasible in motion generation using a PMM motion generator in towing tank. Egeberg *et al.* [2014] investigated the vortices of a surface combatant for static drift angles 0°, 10° and 20° by means of tomographic particle image velocimetry (TPIV) system in a towing tank. However, there are still some obvious deficiencies in model test. The complexity of experimental settings can lead to time consuming and expensive to predict hydrodynamic performance. In addition, there are limitations in obtaining physical understanding of flow field around a ship in model tests, especially for the oblique towed condition.

Numerical simulation methods based on Computational Fluid Dynamics (CFD) for ship maneuverability significantly contribute to resolve the problems. Stern *et al.* [2011] gave an overview of the benchmark cases for the prediction capabilities of different ship maneuver simulation methods for typical tanker, container, and combatant hulls. Bhushan *et al.* [2009] investigated flow field of a fully appended DTMB 5415 at both model scale and full scale using unsteady Reynolds-averaged Navier–Stokes (URANS) method with different wall functions. Wang *et al.* [2011] computed viscous flow around KVLCC2 model using FLUENT, their numerical results agreed well with experimental data in static oblique towed conditions. Hajivand and Mousavizadegan [2015] carried out a numerical maneuvering oblique towed test for a DTMB 5512 model in OpenFOAM. The obtained linear and nonlinear velocity dependent damping coefficients showed good agreement with available experimental data. Detailed validation of the complex free surface flow around a surface combatant DTMB5415 at 20° static drift condition were presented by Visonneau *et al.* [2015] using ISIS-CFD flow solver.

The overset grid approach, composed of blocks of overlapping grids which can move independently, makes it possible to conduct the computation of complex motions. The overset grid approach has been applied to the computation of static and dynamic maneuvers. Using the URANS method with dynamic overset grid technology, Carrica *et al.* [2013] presented numerical results of steady turn and zigzag

for a surface combatant at both model and full scale, which indicated that URANS approach with overset grid technology are feasible for ship maneuvering simulation. Sakamoto *et al.* [2012a, 2012b] performed URANS simulations of the bare hull DTMB 5415 model using the CFD code Ship-Iowa Ver. 4, where the dynamic overset grid method was implemented. Verification and validation for the forces, moments and hydrodynamic derivatives acting on the hull and local flow characteristics were presented. Meng and Wan [2016] investigated the effect of drift angle on viscous flow and hydrodynamical forces of KVLCC2M ship model in both deep and shallow water using overset grid method.

The objective of this work is to investigate hydrodynamic performance and viscous flow field of the DTMB 5512 model at different drift angles. In this paper, the in-house CFD solver naoe-FOAM-SJTU is developed by implementing overset grid technique into the open source code OpenFOAM. An external program Suggar++ [Noack *et al.* (2009)] is used to obtain the grid connectivity among multiple overset component grids. The numerical results of the hydrodynamic forces, moments and the hydrodynamic derivatives are presented and compared with experiments performed by Gui *et al.* [2001a, 2001b]. The physical experiment is carried out by a static PMM system to measure the hydrodynamic loads acting on the hull model. The details information of flow field around ship hull will be given and compared with the available experiment results, which shows that the current approach can be an alternative tool to predict the viscous flow and hydrodynamic loads for oblique towed ships.

2. Numerical Methods

2.1. *naoe-FOAM-SJTU solver*

The CFD solver naoe-FOAM-SJTU is developed for computing viscous flows around ships and ocean structures [Cao and Wan (2014); Shen *et al.* (2014, 2015); Shen and Wan (2014); Wang *et al.* (2015, 2016, 2019)], and mainly composed of a dynamic overset grid module, a 6DoF motion module, a velocity inlet wave-making module and a mooring system module. The CFD solver naoe-FOAM-SJTU solves Navier–Stokes equations for unsteady turbulent flows with VOF method capturing free surface around the ship hull [Wang *et al.* (2017, 2018)].

The URANS equations are adopted to address the unsteady incompressible viscous flow in naoe-FOAM-SJTU solver. The Navier–Stokes equations can be stated as the continuity and the momentum equations, which are listed as follows:

$$\nabla \cdot \mathbf{U} = 0, \tag{1}$$

$$\frac{\partial \rho \mathbf{U}}{\partial t} + \nabla(\rho(\mathbf{U} - \mathbf{U}_g)\mathbf{U}) = -\nabla p_d - \mathbf{g} \cdot \mathbf{x}\nabla\rho$$
$$+ \nabla \cdot (\mu_{\text{eff}}\nabla\mathbf{U}) + (\nabla\mathbf{U}) \cdot \nabla\mu_{\text{eff}} + \boldsymbol{f}_\sigma, \tag{2}$$

where $\boldsymbol{U}$ and $\boldsymbol{U}_g$ are the velocity field and the velocity of grid nodes, respectively. $p_d = p - \rho\mathbf{g}\cdot\mathbf{x}$ is the dynamic pressure and p is the total pressure, ρ is the mixed density with water and air. $\mu_{\mathrm{eff}} = \rho(\nu - \nu_t)$ is the effective dynamic viscosity, in which ν and ν_t are kinematic viscosity and eddy viscosity, respectively. $\boldsymbol{f}_\sigma$ is the surface tension caused by the free surface.

The free surface is captured by VOF method [Hirt and Nichols (1981)] with artificial bounded compression techniques. Each of the two phase in VOF method is considered to have a separately defined volume fraction (α), and the volume fraction function can be determined by solving a transport equation:

$$\frac{\partial\alpha}{\partial t} + \nabla\cdot(\alpha\mathbf{U}) + \nabla\cdot[\alpha(1-\alpha)\boldsymbol{U}_r] = 0. \tag{3}$$

Different phases are marked with volume fraction α, which indicates the relative proportion of fluid in each cell and its value is always between zero and one at interface.

$$\begin{cases} \alpha = 0 & \text{air,} \\ 0 < \alpha < 1 & \text{interface,} \\ \alpha = 1 & \text{water.} \end{cases} \tag{4}$$

Van Leer scheme is applied for VOF equation in OpenFOAM. The RANS and VOF transport equations are discretized by finite volume method (FVM). The PIMPLE algorithm is used to solve the coupled equation of velocity and pressure. The convection terms are solved by a second-order TVD limited linear scheme, and the diffusion terms are approximated by a second-order central difference scheme.

2.2. *Overset grid approach*

An overset grid system is composed of blocks of overlapping grids which can move independently without any constraints. Every grid cell in the computational domain can be marked as fringe, hole or donor. The information of cell types is stored in the domain connectivity information (DCI), which is generated by Suggar++ utility. Suggar++ is capable of providing DCI for node-centered and cell-centered solvers, and can handle structured and unstructured grids. Since OpenFOAM stores information at cell centers and is discretized with unstructured grids, this makes Suggar++ a good candidate for implementation of overset grids.

With the overset grid capability, a full 6DoF motion module with a hierarchy of bodies is implemented, which allows the ship and its appendages to move simultaneously. This module includes two coordinate systems: one is earth-fixed system and the other is ship-fixed system. The earth-fixed system can be fixed to earth or move at a constant speed respect to the ship. The ship-fixed system is fixed to the ship and translates and rotates according to the ship motions. At the initial condition, the two systems are parallel. With the movement of ship, the solver calculates the forces and moments in the earth-fixed system and then transforms them

to ship-fixed system. Details of the 6DoF module with overset grid technique can be found in Shen *et al.* [2015].

3. Geometry and Test Conditions

3.1. *Geometry*

In this work, the bare hull surface combatant DTMB 5512 model was applied to study the effect of drift angle on viscous flow and ship hydrodynamics. Static towed model tests for bare hull DTMB 5512 were carried out in the towing tank by Iowa Institute of Hydraulic Research (IIHR). The scale factor is 1:46.588. The geometry of the DTMB 5512 model is shown in Fig. 1 with main particulars of the DTMB 5512 hull at both full scale and model scale, as shown in Table 1. In order to obtain a mesh with good quality, the sides of hull deck and stern plate are rounded off.

As mentioned in numerical methods part, two coordinate systems are used to solve the 6DoF equations. One is earth-fixed system and the other is ship-fixed system. Figure 2 describes the coordinate systems utilized for the present simulations. In the figure, X_s, Y_s denote the XY-plane in the ship-fixed system, and X_e, Y_e denote the XY-plane in the earth-fixed system. The positive direction of X_e towards to the aft perpendicular and the positive direction of the Y_e is from port to starboard. In this way, the direction of the ship rotation is in clockwise sense with the right-handed coordinate system. During static oblique towed condition, the model is towed at a constant velocity U with the initial drift angle β relative to the ship's axis.

Fig. 1. Geometry of DTMB 5512 model.

Table 1. Main dimensions and particulars.

| Main features	Symbol	Full scale	Model scale
Scale ratio	λ	1	46.588
Length between perpendiculars	L_{pp} (m)	142.00	3.048
Length of waterline	L_{wl} (m)	142.1	3.052
Breadth	B (m)	19.06	0.409
Draught	T (m)	6.150	0.132
Displacement	Δ (kg)	84,244,000	82.600
Wetted surface	S (m^2)	2972.6	1.380
Longitudinal center of gravity	LCG (m)	70.34	1.539
Vertical center of gravity	KG (m)	5.582	0.120
Longitudinal inertia radius	K_{yy} (m)	35.50	0.777
Transverse inertia radius	K_{xx} (m)	7.052	0.131
Metacentric height	GM (m)	1.950	0.096
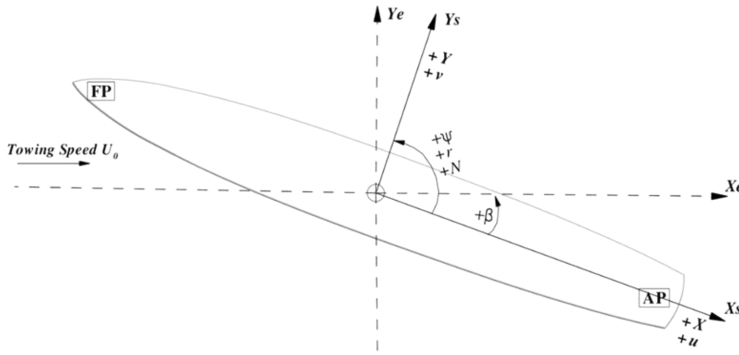
Fig. 2. Coordinate systems of static simulations.

3.2. *Mesh generation*

In this paper, the dynamic overset grid approach is applied for the decomposition of the computational grids, which include two parts, i.e., the background grid and the grid around ship hull. Overlapping areas between the two parts can move independently without restrictions. Connections between the two parts are built by interpolation at appropriate cells or points. Figure 3 shows the arrangement of the computational domain. The background domain extends to $-1.5L_{pp} < x < 5.0L_{pp}$, $-1.5L_{pp} < y < 1.5L_{pp}$, $-1.0L_{pp} < z < 0.5L_{pp}$, and the hull domain is much smaller with a range of $-0.2L_{pp} < x < 1.2L_{pp}$, $-0.2L_{pp} < y < 0.2L_{pp}$, $-0.1L_{pp} < z < 0.1L_{pp}$. The boundary conditions are as following: At the inlet, fixed value condition, Dirichlet condition is adopted. At the outlet, zero Gradient condition is applied for both velocity and pressure. The farfield is set as symmetry
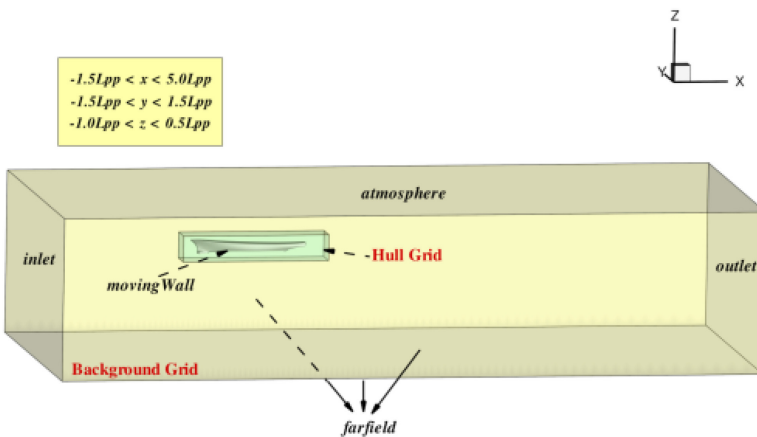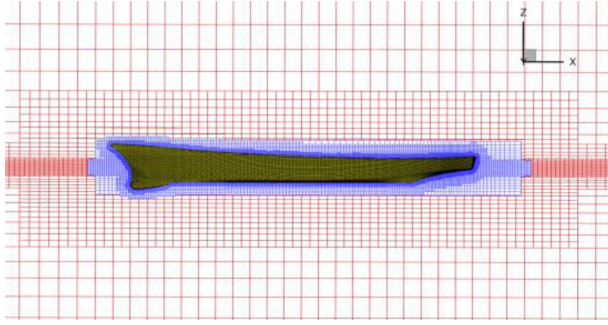
Fig. 3. Computational domain.

Fig. 4. (Color online) Overset grid distribution (Blue grid stands for hull grid, and red grid stands for background grid).

plane. For ship hull boundaries, movingWallVelocity is applied for velocity condition and buoyant pressure is applied for pressure condition.

An automatic mesh-generation tool *snappyHexMesh* was applied to generate the meshes for the computation. The total cell number is 1.89 M with hull grid 0.68 M and background grid 1.21 M. By using overset grid technique, all the cases carried out in this paper are applying a same grid arrangement except for the convergence study, where three kind of grids are chosen with a scaling factor $\sqrt{2}$. The local mesh distribution around the ship hull is shown in Fig. 4. For drift cases, the grid around hull was rotated to aimed angle. To make it easy to converge in each time step, the interface Courant number was controlled to be under 0.3. The time step is 0.001 s in each case.

3.3. *Case conditions*

The numerical computations in this study were set up according to experimental with a 46.588 scale model of the bare hull DTMB 5512 by Gui *et al.* [2001a, 2001b] and Longo and Stern [2005]. Straight-ahead test at constant velocity U is first simulated for validation of present solver. The ship speed is $U = 1.531$ m/s with the corresponding Froude number $F_r = 0.28$ and the Reynolds number Re $= 4.67 \times 10^6$. During the static drift test, the ship model is towed with different drift angle β with respected to the ship towing direction. The drift angles are $\beta = 0°$, $6°$, $10°$, $12°$, $16°$, $20°$, respectively. The ship model is subjected to the given motion and free to trim and sinkage. The general plan was to investigate the effect of the drift angle on hydrodynamic quantities.

4. Results and Discussion

All the numerical results and analysis are based on the nondimensional parameters, which are made by towing speed U, model length L_{pp}, draft T, fluid density ρ, gravitational acceleration g and the dynamic viscosity μ. The nondimensional expressions for Froude and Reynold number are $F_r = U/\sqrt{gL_{pp}}$ and $R_e = \rho U L_{pp}/\mu$.

Other nondimensional forms of v', $\dot{v}'$, r', $\dot{r}'$, X', Y', N' are as follows:

$$\begin{bmatrix} v' \\ \dot{v}' \end{bmatrix} = \begin{bmatrix} \dfrac{v}{U} \\ \dfrac{\dot{v}}{U} \end{bmatrix},$$ (5)

$$\begin{bmatrix} r' \\ \dot{r}' \end{bmatrix} = \begin{bmatrix} \dfrac{rL_{pp}}{U} \\ r\left(\dfrac{L_{pp}}{U}\right)^2 \end{bmatrix},$$ (6)

$$\begin{bmatrix} X' \\ Y' \\ N' \end{bmatrix} = \begin{bmatrix} \dfrac{X}{0.5\rho U^2 T L_{pp}} \\ \dfrac{Y}{0.5\rho U^2 T L_{pp}} \\ \dfrac{N}{0.5\rho U^2 T L_{pp}^2} \end{bmatrix}.$$ (7)

In this study, the hydrodynamic forces and moments in Eq. (7) are very important for further analysis. According to Maneuvering Modeling Group (MMG) model, the forces and moment coefficients in ship-fixed system of the bare hull model are described as follows:

$$\begin{bmatrix} X' \\ Y' \\ N' \end{bmatrix} = \begin{bmatrix} X_* + X_{vv}v'^2 + X_{rr}r'^2 + X_{vr}v'r' \\ Y_{\dot{v}}\dot{v}' + Y_{\dot{r}}\dot{r}' + Y_v v' + Y_{v|v|}v'|v'| + Y_r r' + Y_{r|r|}r'|r'| \\ \quad + Y_{|v|r}|v'|r' + Y_{v|r|}v'|r'| \\ N_{\dot{v}}\dot{v}' + N_{\dot{r}}\dot{r}' + N_v v' + N_{v|v|}v'|v'| + N_r r' + N_{r|r|}r'|r'| \\ \quad + N_{|v|r}|v'|r' + N_{v|r|}v'|r'| \end{bmatrix}.$$ (8)

For the static drift tests, the ship model has no angular velocity r and the forces and moment coefficients on the right hand of Eq. (8) can be simplified as follows:

$$\begin{bmatrix} X' \\ Y' \\ N' \end{bmatrix} = \begin{bmatrix} X_* + X_{vv}v'^2 \\ Y_v v' + Y_{v|v|}v'|v'| \\ N_v v' + N_{v|v|}v'|v'| \end{bmatrix},$$ (9)

where X_* is the towing force with no drift angle.

4.1. *Grid convergence study*

Grid convergence study is a straight and consistent way to determine the magnitude of discretization error in numerical simulation. In this paper, grid convergence examinations are performed for the cases of the straight-ahead towed condition. This study is also necessary for the numerical computation and determine which

grid is suitable for the simulation. All grids used in this paper are unstructured of which systematic refinement in three directions is difficult. In order to achieve consistent refinement in all directions, the following approach is applied. *Snappy-HexMesh* requires a preliminary Cartesian grid and splits cells from it to get an unstructured mesh. By creating systematically refined Cartesian grids with a specific refinement ratio and running *SnappyHexMesh* over these grids, the resulting unstructured grids are approximately systematically refined as required. According to the experiments, the errors arising from extrapolation can be reduced if the refinement ratio of $r > 1.3$ [Hajivand and Mousavizadegan (2015)]. In this study, a refinement ratio of $r = \sqrt{2}$ in each direction is selected. The number of meshes and calculated nondimensional force coefficients are shown in Table 2.

Stern *et al.* [2006] proposed a verification method to estimating uncertainty due to grid and time step errors. The convergence solution (R_G) of different solutions (S_i) is defined as follows:

$$R_G = \frac{S_2 - S_1}{S_3 - S_2}, \tag{10}$$

where S_i corresponds to solutions with fine, medium and coarse grid, respectively. Different R_G values represent different convergence conditions: (1) $0 < R_G < 1$ represents monotonic convergence, and generalized Richardson extrapolation (RE) is used to estimate grid uncertainty. (2) $R_G < 0$ represents oscillatory convergence, and uncertainties can be estimated by attempting to bound the error based on oscillation maximums S_U and minimums S_L. (3) $R_G > 1$ represents divergence, and uncertainties cannot be estimated. The grid convergence study is conducted at $F_r = 0.28$ with three sets of grid number ranging from 0.64 million to 3.67 million. The results show good convergence, as summarized in Table 2. As the grid is refined, the total resistance coefficient approaches the experimental data monotonically. Thus, the RE method is used to estimate convergence rate in this study [Roache (1994)]. Order of discretization is estimated as follows:

$$P = \frac{\ln(1/R_G)}{\ln(r)}, \tag{11}$$

Table 2. Grid convergence study.

Grid	ID	Grid size	C_p	C_v	C_t	Error of C_t
EFD					1.706×10^{-2}	
Fine	S1	3.67M	0.507×10^{-2}	1.171×10^{-2}	1.678×10^{-2}	-1.66%
Medium	S2	1.87M	0.499×10^{-2}	1.162×10^{-2}	1.661×10^{-2}	-2.64%
Coarse	S3	0.64M	0.473×10^{-2}	1.124×10^{-2}	1.597×10^{-2}	-6.39%
R_G			0.307	0.237	0.265	
P			3.4088	4.1559	3.834	
GCI_{12}			0.87\%	0.31\%	0.45\%	
GCI_{23}			2.88\%	1.27\%	1.74\%	
Convergence type			Monotonic	Monotonic	Monotonic	

then, Grid Convergence Index (GCI) is defined as follows:

$$\mathrm{GCI}_{ij} = F_S \frac{|e_{ij}|}{r^p - 1}, \tag{12}$$

where F_S is a safety factor, and for convergence study with minimum three grids or more, $F_S = 1.25$ according to Roache [1994], e_{ij} is the error between S_i and S_j. The GCI can indicate the error using different grids. Small value of GCI means the solution is accurate relatively. Table 2 shows the GCI values of different hydrodynamic force coefficients. All coefficients show monotonic convergence with R_G of 0.307, 0.237 and 0.265, respectively. The GCI_{12} (between fine and medium) of the total resistance coefficient C_t is only 0.45%, which can illustrate that grid density has limited effect on resistance in fine and medium grid. The GCI of C_p shows the maximum values. It is obvious that the values of GCI_{23} (between medium and coarse) are larger than those of GCI_{12} and the error of C_t between coarse grid and experimental results is much larger than that of medium and fine grid. The grid uncertainty between the simulation results of fine grid and medium grid is under 1%, but the computational time is significantly increased. Therefore, the medium grid is selected in our following numerical computations of obliquely towed conditions.

4.2. *Straight-ahead case and validation*

For the calculation of straight-ahead case, comparisons were made with the experiments performed by Gui *et al.* [2001a, 2001b]. The force coefficients are defined as follows:

$$\begin{bmatrix} C_t \\ C_v \\ C_p \end{bmatrix} = \begin{bmatrix} \dfrac{R_T}{0.5\rho U^2 T L_{pp}} \\ \dfrac{R_V}{0.5\rho U^2 T L_{pp}} \\ \dfrac{R_P}{0.5\rho U^2 T L_{pp}^2} \end{bmatrix}, \tag{13}$$

where ρ is fluid density, TL_{pp} is lateral underwater area and U is the ship speed. As shown in Table 3, the total resistance coefficient C_t of CFD and EFD is 1.661×10^{-2} and 1.706×10^{-2}, respectively. The predicted result is underestimated by 2.64%, which indicates that the present approach can give accurate prediction of the ship resistance. Predicted motion is also presented in Table 3. The errors of predicted sinkage and trim are 0.75% and 5.96%, respectively.

Furthermore, CFD approach cannot only give the prediction of ship motions and forces, but also the whole flow information around the ship hull. The predicted wave pattern and wake field are presented and compared with the experiment measurements [Gui *et al.* (2001a, 2001b)]. Figure 5 shows the comparison of wave pattern between this work and experimental results, where $Z(m)$ stands for the wave elevation. It is obvious that the predicted bow wave and stern wave crest match fairly

Table 3. Total resistance comparison between CFD and EFD.

Parameters	CFD	EFD	Error
sinkage (m)	-5.32×10^{-3}	-5.36×10^{-3}	0.75%
Pitch (degree)	-0.103	-0.0972	5.96%
C_p	0.499×10^{-2}		
C_v	1.162×10^{-2}		
C_t	1.661×10^{-2}	1.706×10^{-2}	-2.64%
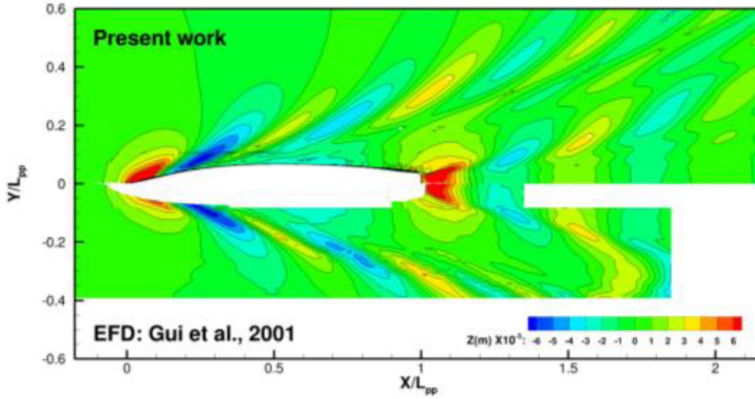
Fig. 5. Comparison of wave pattern between present work and experiment.

well with the available measurements. In addition, the scattered wave and shear wave also show good consistence with the experiment.

Comparison of wake region at longitudinal section of $x = 0.935\ L_{pp}$ between this work and experiment is presented in Fig. 6. The distribution of nondimensional mean velocity U_m/U shows consistent tendency with experimental data. However, discrepancies can be observed for the local velocity distribution. CFD result shows a pattern of relatively thicker boundary layer near the waterplane, but thinner near mid plane. This may be due to viscous modeling using RANS approach. Applying more accurate turbulence models maybe an efficient way to improve the computational results according to previous results in Gothenburg 2010 CFD Workshop [Toxopeus *et al.* (2011)]. Good agreements are achieved for both wave pattern and the wake region, showing that present numerical method is suitable to study the viscous flow around the hull and can lay a good foundation for the prediction of oblique towed conditions.

4.3. *Static drift*

4.3.1. *Forces and moments*

Figure 7 shows the experimental and computational results of nondimensional forces and moment coefficients at different drift angles. We can see that the computational
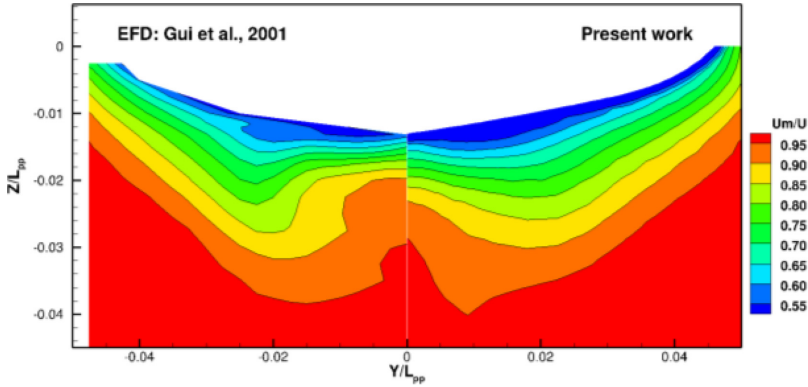
Fig. 6. Comparison of wake region at longitudinal section of $x = 0.935\ L_{pp}$ between present work and experiment.
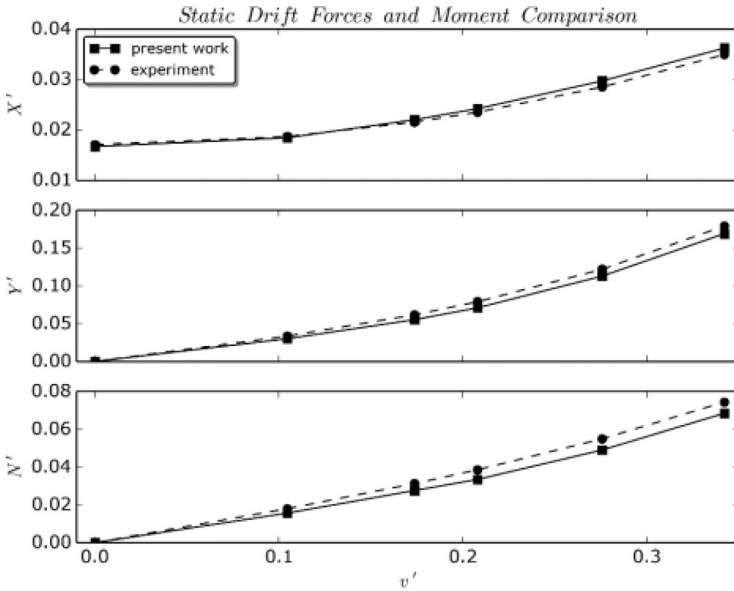

Fig. 7. Forces and moment coefficients for static drift at different drift angles.

results show an overall agreement with the experimental data. The error increases with the growing of drift angle and the difference between computational results and experimental data for the longitudinal forces varies from 1.28% to 4.35%. As for the lateral forces, the error varies from 5.66% to 10.55%. The predicted yaw moments experience the same trend. While the error between predicted results and experimental results is up to 11% when the drift angle varies from 0° to 10° and

it tends to become larger when the drift angle increases. The predicted forces and moment show less accuracy at larger drift angle.

According to Eq. (7), the hydrodynamic derivatives can be obtained using the least square method. The obtained results as well as the error between the hydrodynamic derivatives obtained from computational results and the experimental data are given in Table 4. For all derivatives, the CFD results were underpredicted compared with the experiment. Linear derivatives were more accurate than that of the nonlinear ones with errors up to 6.21% and 9.95%, respectively. This indicates that the current approach can be an alternative way to predict the static hydrodynamic derivatives.

4.3.2. *Wave pattern*

The wave pattern is a significant factor that illustrates the hydrodynamic performance of a ship, especially for the wave making resistance. Wave patterns are shown in Fig. 8 with the drift angle of $\beta = 0°$, $6°$, $10°$, $20°$. The contours in the figure are colored by wave elevations. With the variation of the drift angle, the wave pattern around the hull shows strong asymmetry. The wave amplitude increases at the windward side and decreases at the leeward side. The trough at the leeward side becomes more obvious and the wave elevation sheds diverging waves away from the hull. The different distribution in wave elevation will lead to pressure redistribute around ship hull, which will further affect the hydrodynamic performance, especially for the lateral force and yaw moment.

Unlike the straight-ahead condition, there is no available measurement result for the flow field including the wave pattern and wake flow. Here, we only compared the different hydrodynamic characteristics. In order to give quantitively analysis of the wave pattern at different drift angles, we have measured the wave angle at different conditions. For the straight-ahead condition, the angle is the Kelvin angle of 19.28. While for the obliquely towed cases, the divergent waves and transverse waves are more complicated with strong interactions. Therefore, there is no standard Kelvin wave envelope. The wave-making angle θ is then measured by the direction

Table 4. Hydrodynamic derivatives from static drift tests.

Derivatives	CFD	EFD*	Error
X'_{vv}	0.157	0.162	3.09%
Y'_{v}	0.187	0.197	5.08%
$Y'_{v|v|}$	0.896	0.949	5.58%
N'_{v}	0.136	0.145	6.21%
$N'_{v|v|}$	0.190	0.211	9.95%

Note: *EFD results are obtained by the same procedure as CFD.

(a) $\beta = 0°$

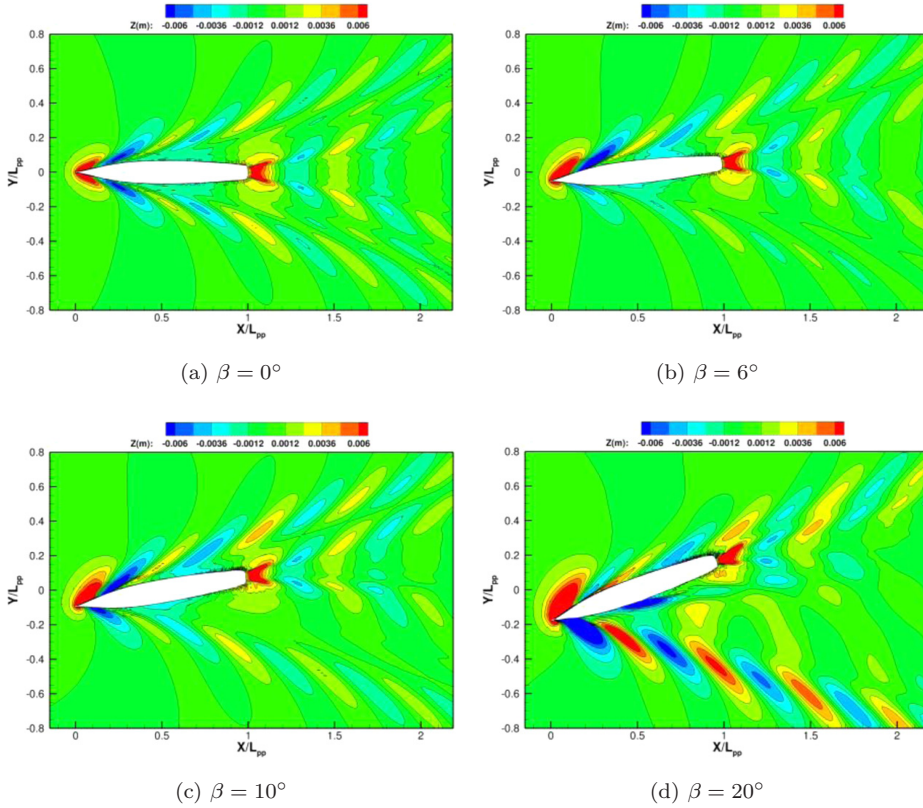(b) $\beta = 6°$

(c) $\beta = 10°$

(d) $\beta = 20°$

Fig. 8. Comparison of wave pattern at different drift angle.

of divergent waves and the longitudinal direction of ship hull as shown in Fig. 9. It is obvious that wave angle becomes larger with the increase of drift angle. Wave angle $\theta = 22°$, $27°$, $36°$ for 6, 10, 20 drift angles, respectively.

4.3.3. *Wake region*

Apart from the wave patterns, the wake flows in the aft region are also presented to see the difference with drift angles. Figure 10 illustrates the wake region around the hull at longitudinal section of $x = 0.935 \ L_{pp}$ for different drift angles, i.e., $\beta = 0°$, $6°$, $10°$, $20°$. All the figures are captured at stable condition to get effective flow information. The velocity components are nondimensioned by the ship speed U and the ship length L_{pp}. It can be found that velocity contours show much difference. As the drift angle increases, the flow field shows a growing asymmetry phenomenon. At drift angle $\beta = 0°$, the wake region around ship hull is very tight, while at $\beta = 6°$, the wake region becomes larger and extends to the opposite direction. With the increase of drift angle, the wake region, represented by the wake fraction $\omega = (U - Ux)/U$, can be extended to a wider area both in transverse direction
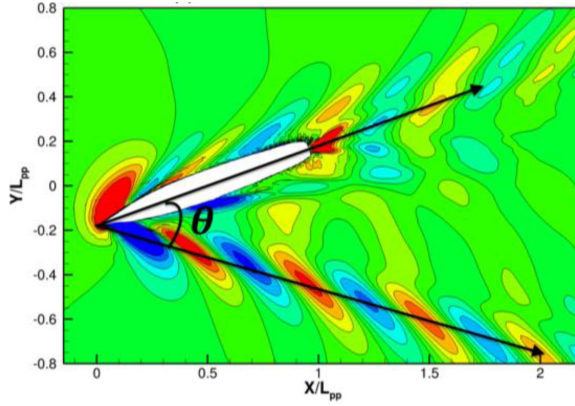
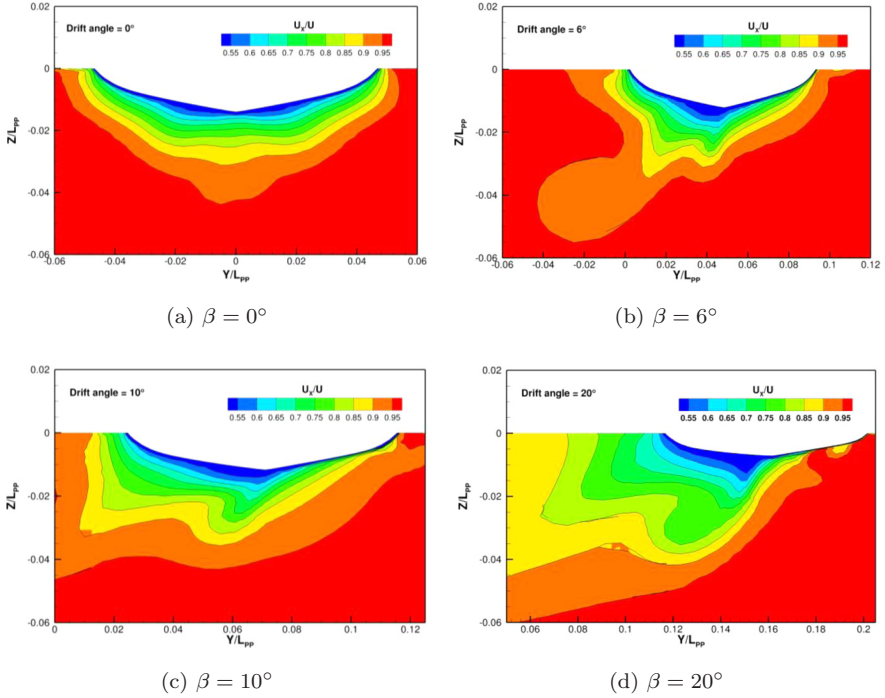Fig. 9. Schematic of wave angle in obliquely towed condition.

(a) $\beta = 0°$

(b) $\beta = 6°$

(c) $\beta = 10°$

(d) $\beta = 20°$

Fig. 10. Wake region at longitudinal section of $x = 0.935\ L_{pp}$ (view from fore. to aft.)

and vertical direction. It can be noted that the wake fraction of $\omega = 0.1$ can be extended to $Z/L_{pp} > 0.045$ at $\beta = 20°$, while it is less than 0.03 in the straight-ahead condition. Since we are using RANS approach with very coarse grid, it is difficult to resolve the very detailed flow behavior. Futurework will focus on more

accurate turbulent model and larger grid to give more reliable prediction of the flow field.

5. Conclusions

This paper presents numerical simulation of the obliquely towed surface combatant DTMB 5512 using URANS method with dynamic overset grid. Simulations at six different drift angles are performed by the CFD solver naoe-FOAM-SJTU. Grid convergence study with three sets of grids is conducted and it shows the medium grid can give good prediction with a lower computational cost. Straight-ahead condition is carried out to validate the capability of the present solver for predicting hydrodynamic forces and viscous flow field. Predicted total resistance is compared with the experimental results and the error is only -2.64%, which implies the present solver is capable of predicting the hydrodynamic forces acting on ship moving obliquely. In addition, the wave pattern and wake field also show good agreement with experimental data. For static drift tests, the lateral force, yaw moment and the derived hydrodynamic derivatives are presented and compared with the experimental results. The overall trend of the lateral force and yaw moment show fair agreement with the experimental data. The derived hydrodynamic derivatives show good agreement to the experimental data with the error under 10%. According to the results, the average error of nonlinear derivatives is larger than that of linear derivatives. Wave patterns and wake regions around the hull at different drift angles are also presented and analyzed. Flow visualizations give a better description of the hydrodynamic performance during the oblique towed conditions. Future work will mainly focus on more accurate turbulence model and larger grid number to give better prediction of the detailed wake flows in large drift angles.

Acknowledgments

References

Bhushan, S., Xing, T., Carrica, P. M. and Stern, F. [2009] "Model-and full-scale URANS simulations of Athena resistance, powering, seakeeping, and 5415 maneuvering," *J. Ship Res.* **53**(4), 179–198, https://www.researchgate.net/profile/Tao_Xing/publication/233670398_Model-_and_Full-Scale_URANS_Simulations_of_Athena_Resistance_Powering_Seakeeping_and_5415_Maneuvering/links/55269fb70cf2f6e65169bdfc.pdf.

Cao, H. J. and Wan, D. C. [2014] "Development of multidirectional nonlinear numerical wave tank by naoe-FOAM-SJTU solver," *Int. J. Ocean Syst. Eng.* **4**(1), 52–59, doi:10.5574/IJOSE.2014.4.1.049.

Carrica, P. M., Ismall, F., Hyman, M., Bhushan, S. and Stern, F. [2013] "Turn and zigzag maneuvers of a surface combatant using a URANS approach with dynamic overset grids," *J. Mar. Sci. Technol.* **18**(2), 166–181, doi:10.1007/s00773-012-0196-8.

Egeberg, T. F., Yoon, H., Stern, F., Pettersen, B. and Bhushan, S. [2014] "Vortex shedding from a ship hull by means of tomographic PIV," 2014 *the* 33*rd Int. Conf. Ocean, Offshore and Arctic Engineering*, San Francisco, USA, pp. 1–11, doi:10.1115/OMAE2014-23357.

Gui, L., Longo, J. and Stern, F. [2001a] "Towing tank PIV measurement system, data and uncertainty assessment for DTMB Model 5512," *Exp. Fluids* **31**(3), 336–346, doi:10.1007/s003480100293.

Gui, L., Longo, J. and Stern, F. [2001b] "Biases of PIV measurement of turbulent flow and the masked correlation-based interrogation," *Exp. Fluids* **30**, 27–35, doi:10.1007/s003480000131.

Hajivand, A. and Mousavizadegan, S. H. [2015] "Virtual maneuvering test in CFD media in presence of free surface," *Int. J. Nav. Arch. Ocean Eng.* **7**(3), 540–558, doi:10.1515/ijnaoe-2015-0039.

Hirt, C. W. and Nichols, B. D. [1981] "Volume of fluid (VOF) method for the dynamic of free boundaries," *J. Comput. Phys.* **39**, 201–225, doi:10.1016/0021-9991(81)90145-5.

Longo, J. and Stern, F. [2005] "Uncertainty assessment for towing tank tests with example for surface combatant DTMB model 5415," *J. Ship Res.* **49**(1), 55–68, http://www.ivt.ntnu.no/imt/courses/tmr7/resources/Stern_uncertainty_anal_JSR.pdf.

Meng, Q. J. and Wan, D. C. [2016] "Numerical simulations of viscous flow around the obliquely towed KVLCC2M model in deep and shallow water," *J. Hydrodyn. Ser. B* **28**(3), 506–518, doi:10.1016/S1001-6058(16)60655-8.

Noack, R. W., Boger, D. A., Kunz, R. F. and Carrica, P. M. [2009] "Suggar++: An improved general overset grid assembly capability," 2009 *the* 47*th AIAA Aerospace Science and Exhibit*, San Antonio, USA, pp. 22–25, http://arc.aiaa.org/doi/pdf/10.2514/6.2009-3992.

Roache, P. J. [1994] "Perspective: A method for uniform reporting of grid refinement studies," *J. Fluids Eng.* (*ASME*) **116**, 405–413, doi:10.1115/1.2910291.

Sakamoto, N., Carrica, P. M. and Stern, F. [2012a] "URANS simulations of static and dynamic maneuvering for surface combatant: Part 1. Verification and validation for forces, moment, and hydrodynamic derivatives," *J. Mar. Sci. Technol.* **17**(4), 422–445, doi:10.1007/s00773-012-0178-x.

Sakamoto, N., Carrica, P. M. and Stern, F. [2012b] "URANS simulations of static and dynamic maneuvering for surface combatant: Part 2. Analysis and validation for local flow characteristics," *J. Mar. Sci. Technol.* **17**(4), 446–468, doi:10.1007/s00773-012-0184-z.

Shen, Z. R., Carrica, P. M. and Wan, D. C. [2014] "Ship motions of KCS in head waves with rotating propeller using overset grid method," 2014 *the* 33*rd Int. Conf. Ocean, Offshore and Arctic Engineering*, San Francisco, USA, pp. 1–8, doi:10.1115/OMAE2014-23657.

Shen, Z. R. and Wan, D. C. [2014] "Computation of steady viscous flows around ship with free surface by overset grids techniques in OpenFOAM," 2014 *the Twenty-Fourth Int. Ocean and Polar Engineering Conf.*, Busan, Korea, pp. 832–838. Document ID: ISOPE-I-14-309, https://www.onepetro.org/conference-paper/ISOPE-I-14-309.

Shen, Z. R., Wan, D. C. and Carrica, P. M. [2015] "Dynamic overset grids in OpenFOAM with application to KCS self-propulsion and maneuvering," *Ocean Eng.* **108**, 287–306, doi:10.1016/j.oceaneng.2015.07.035.

Stern, F., Agdrup, K., Kim, S. Y., Hochbaum, A. C., Rhee, K. P., Quadvlieg, F. A. and Gorski, J. [2011] "Experience from SIMMAN2008-The first workshop on verification and validation of ship maneuvering simulation methods," *J. Ship Res.* **55**(2), 135–147, http://www.ingentaconnect.com/content/sname/jsr/2011/00000055/00000002/art00005.

Stern, F., Wilson, R. and Shao, J. [2006] "Quantitative V&V of CFD simulations and certification of CFD codes," *Int. J. Numer. Methods Fluids* **50**(11), 1335–1355, doi:10.1002/fld.1090.

Toxopeus, S. L., Simonsen, C. D., Guilmineau, E., Visonneau, M., Xing, T. and Stern, F. [2011] "Viscous-flow calculations for KVLCC2 in manoeuvring motion in deep and shallow water," *AVT-189 Specialists Meeting on Assessment of Stability and Control Prediction Methods for NATO Air and Sea Vehicles*, Portsdown West, UK, pp. 151–169, doi:10.1007/978-94-007-6143-8_9.

Visonneau, M., Guilmineau, E., Wackers, J., Deng, G. and Queutey, P. [2015] "Assessment of statistical and hybrid LES turbulence closures for surface combatant DTMB 5415 at 20° static drift condition," *2015 the 34th Int. Conf. Ocean, Offshore and Arctic Engineering.* St. John's, Canada, pp. V011T12A021–V011T12A021, doi:10.1115/OMAE2015-41372.

Wang, J. H., Liu, X. J. and Wan, D. C. [2015] "Numerical simulation of an oblique towed ship by naoe-FOAM-SJTU solver," *2015 the Twenty-Fifth Int. Ocean and Polar Engineering Conf.*, Hawaii, USA, pp. 432–438. Document ID: ISOPE-I-15-010, https://www.onepetro.org/conference-paper/ISOPE-I-15-010.

Wang, J. H., Liu, X. J., Wan, D. C. and Chen, G. [2016] "Numerical prediction of KCS self-propulsion in shallow water," *2016 the Twenty-Sixth Int. Ocean and Polar Engineering Conf.*, Rhodes, Greece, pp. 757–763. Document ID: ISOPE-I-16-034, https://www.onepetro.org/conference-paper/ISOPE-I-16-034.

Wang, J. H. and Wan, D. C. [2016] "Numerical simulation of pure yaw motion using dynamic overset grid technology," *Chin. J. Hydrodyn.* **31**(5), 567–574, doi:10.16076/j.cnki.cjhd.2016.05.006.

Wang, H. M., Xie, Y. H., Liu, J. M., Zou, Z. J. and He, W. [2011] "Experimental and numerical study of hydrodynamic forces on ship in oblique motion," 2011 *Remote Sensing, Environment and Transportation Engineering* (*RSETE*), Nanjing, China, pp. 328–331, doi:10.1109/RSETE.2011.5964280.

Wang, J. H., Zhao, W. W. and Wan, D. C. [2019] "Development of naoe-FOAM-SJTU solver based on OpenFOAM for marine hydrodynamics," *J. Hydrodyn.* **31**(1), 1–20, doi:10.1007/s42241-019-0020-6.

Wang, J. H., Zou, L. and Wan, D. C. [2017] "CFD simulations of free running ship under course keeping control," *Ocean Eng.* **141**, 450–464, doi:10.1016/j.oceaneng.2017.06.052.

Wang, J. H., Zou, L. and Wan, D. C. [2018] "Numerical simulations of zigzag maneuver of free running ship in waves by RANS-overset grid method," *Ocean Eng.* **162**, 55–79, doi:10.1016/j.oceaneng.2018.05.021.